Theor Chem Account (2009) 122:107–114
DOI 10.1007/s00214-008-0490-z

REGULAR ARTICLE

Theoretical studies on the reactions OH + CH_3COCCl_2X (X = F, Cl, Br)

Hui Zhang · Gui-ling Zhang · Jing-yao Liu · Cheng-yang Liu · Bo Liu · Ze-sheng Li

Received: 29 June 2008 / Accepted: 3 November 2008 / Published online: 20 November 2008

Abstract Theoretical investigations are carried out on the title reactions by means of the direct dynamics method. The optimized geometries, frequencies and minimum energy path are obtained at the MP2/6-31 + G(d,p) level, and energetic information is further refined at the MC-QCISD (single-point) level. The rate constants for both reactions are calculated by the improved canonical variational transition state theory with the small-curvature tunneling correction in a wide temperature range 200–3,000 K. The theoretical rate constant is in good agreement with the available experimental data. Furthermore, the effects of different halogen substitution on the rate constants are also discussed.

1 Introduction

Acetone represents an important class of oxygenated volatile organic compounds (VOCs), which are emitted from a variety of anthropogenic and natural sources into the atmosphere. In addition to these direct emissions, atmospheric oxidation of volatile hydrocarbons constitutes a significant source of various ketones. In the degradation of non-halogenated hydrocarbons, acetone is known to be long-lived (several months) [1]. The accumulation of acetone in the upper troposphere and lower stratosphere has recently been highlighted [2–8]. Acetone has been shown to be a potentially important source of OH and HO_2 radicals, resulting in an increased ozone production. Hence, there is a particular need to investigate the chemistry of some halogenated acetones. The most likely fate of halogenated acetones in the Earth's atmosphere would be their reaction with the OH radical. However, there are very limited experimental values available in the literature concerning rate constants of the title reactions. For the reaction OH + CH_3COCCl_3, only Carr et al. [9] measured a rate constant, which is $(1.5 \pm 0.3) \times 10^{-14}$ $cm^3molecule^{-1}$ s^{-1} at 298 K. There are no experimental rate constants available for the reactions OH + CH_3COCCl_2F and OH + CH_3COCCl_2Br. No Arrhenius parameters were reported for these three reactions.

The aim of this paper is to make a systematic theoretical investigation of the kinetic properties of the reactions OH + $CH_3COCCl_2F \rightarrow CH_2COCCl_2F + H_2O$ (R1), OH + $CH_3COCCl_3 \rightarrow CH_2COCCl_3 + H_2O$ (R2), and OH + $CH_3COCCl_2Br \rightarrow CH_2COCCl_2Br + H_2O$ (R3). In addition, because the temperature determined in the experiment is mostly in the lower temperature range of practical interest, theoretical investigation is desirable to give a further understanding and to evaluate the rate constants at high temperatures. To the best of our knowledge, little theoretical work has addressed these reactions.

Here, the dual-level direct dynamics method [10–12] proposed by Truhlar et al. is employed to study the kinetic nature of both reactions. The potential energy surface information, including geometries, energies, gradients, force constants of all the stationary points (reactants, products, and saddle points) and some extra points along

H. Zhang · G.-l. Zhang · C.-y. Liu · B. Liu (✉)
College of Chemical and Environmental Engineering,
Harbin University of Science and Technology,
150080 Harbin, People's Republic China
e-mail: hust_zhanghui1@hotmail.com

J.-y. Liu · Z.-s. Li
Institute of Theoretical Chemistry,
State Key Laboratory of Theoretical
and Computational Chemistry, Jilin University,
130023 Changchun, People's Republic China

the minimum energy path (MEP) are obtained directly from electronic structure calculations. Single-point energies are further carried out at the MC-QCISD level [13]. Subsequently, by means of POLYRATE 9.1 program [14], the rate constants are calculated using the variational transition state theory (VTST) proposed by Truhlar et al. [15, 16]. The comparison between theoretical and experimental results is discussed.

2 Computational method

In the present work, the equilibrium geometries and frequencies of all the stationary points (reactants, products, and saddle points) are optimized at the restricted or unrestricted second-order Møller–Plesset perturbation (MP2) [17–19] level with the 6-31+G(d,p) basis set. The MEP is obtained by intrinsic reaction coordinate (IRC) theory in mass-weighted Cartesian coordinates with a gradient step-size of 0.05 $(\text{amu})^{1/2}$ bohr. Then, the energy derivatives including gradients and Hessians are obtained by calculating the curvature of the reaction path and the generalized vibrational frequencies along the reaction path. In order to obtain more accurate energies and barrier heights, a dual-level direct dynamics method [10–12] is applied to study the title reaction. Single-point energies are refined by the multi-coefficient correlation method based on quadratic configuration interaction with single and double excitations MC-QCISD [13] and on the MP2/6-31+G(d,p) geometries. All the electronic structure calculations are performed by means of the GAUSSIAN03 program package [20].

Variational transition state theory [15, 16] is employed to calculate the rate constants by the POLYRATE 9.1 program [14]. The improved canonical variational transition state theory [21] incorporating small-curvature tunneling (SCT) [22, 23] contributions proposed by Truhlar et al. is applied to evaluate the theoretical rate constants. The improved canonical variational transition state theory rate constants, $k^{\text{ICVT}}(T)$, which can be obtained by minimizing the improved generalized transition state theory rate constant, $k^{\text{IGT}}(T, s)$, at fixed temperature (T) with respect to the dividing surface at s, can be expressed as

$$k^{\text{ICVT}}(T) = \min_{s} k^{\text{IGT}}(T, s).$$

And the improved generalized transition state theory rate constant k^{IGT} for temperature T with respect to the dividing surface at s can be expressed as

$$k^{\text{IGT}}(T, s) = \frac{\sigma Q^{\text{IGT}}(T, s)}{\beta h Q^{R}(T)} \exp(-\beta V_{\text{MEP}}(s)),$$

where s is the location of the improved generalized transition state on the IRC; σ is the symmetry factor accounting for the possibility of two or more symmetry-related reaction paths; β equals $(k_B T)^{-1}$, with k_B being the Boltzmann's constant, h is Planck's constant; $Q^{R}(T)$ is the reactant's partition function per unit volume, excluding symmetry numbers for rotation; $V_{\text{MEP}}(s)$ is the classical energy along the MEP; and $Q^{\text{IGT}}(T, s)$ is the partition function of the improved generalized transition state at s along the MEP. To include the tunneling effect, the ICVT rate constant is multiplied by a transmission coefficient computed with the SCT [22, 23] approximation, which is denoted by $k^{\text{ICVT/SCT}}(T)$. For the title reaction, most of the vibrational modes were treated as quantum-mechanical separable harmonic oscillators except for a few lower vibrational modes. The hindered-rotor approximation of Truhlar and Chuang [24, 25] is used for calculating the partition function of these modes. The model used for hindered rotor approximation is the torsional mode. Here, we use the RW scheme, where R stands for applying the rectilinear model for calculating the reduced moment of inertia (I_j) of the rotator and the W means using the rotational barrier height (W_j) from direct ab initio calculation to estimate the vibrational frequency (ω_j). The vibrational frequency can be estimated by $\omega_{\text{j}} = (W_j/2I_j)^{1/2}M$, where M is the total number of minima along the torsional coordinate in the range 0–2π. In this paper, the values of W_j and M are 1,000 cm^{-1} and 1, respectively. In addition, we used "full" approximation level to calculate the partition function. The two electronic states for OH radicals in the calculation of its electronic partition functions, with a 140 cm^{-1} splitting, are considered. The vibrational frequencies along the reaction path are calculated using redundant rectilinear coordinates. The symmetry factor $\sigma = 3$ for the reaction channels R1, R2, and R3 are taken into account in the rate constant calculation. The curvature components are calculated by using a quadratic fit to obtain the derivative of the gradient with respect to the reaction coordinate.

3 Results and discussions

3.1 Stationary points

The optimized geometric parameters of the reactants (CH_3COCCl_2F, CH_3COCCl_3, CH_3COCCl_2Br, and OH), products (CH_2COCCl_2F, CH_2COCCl_3, CH_2COCCl_2Br, and H_2O), and saddle points (TS1, TS2, and TS3) calculated at the MP2/6-31+G(d,p) level along with the available experimental data [26, 27] are presented in Fig. 1. It can be seen that the theoretical geometric parameters of OH and H_2O are in good agreement with the corresponding experimental values [26, 27]. In TS1, TS2, and TS3 structures, the breaking bonds C–H increase by 11, 11, and 11% compared to the regular bond lengths in

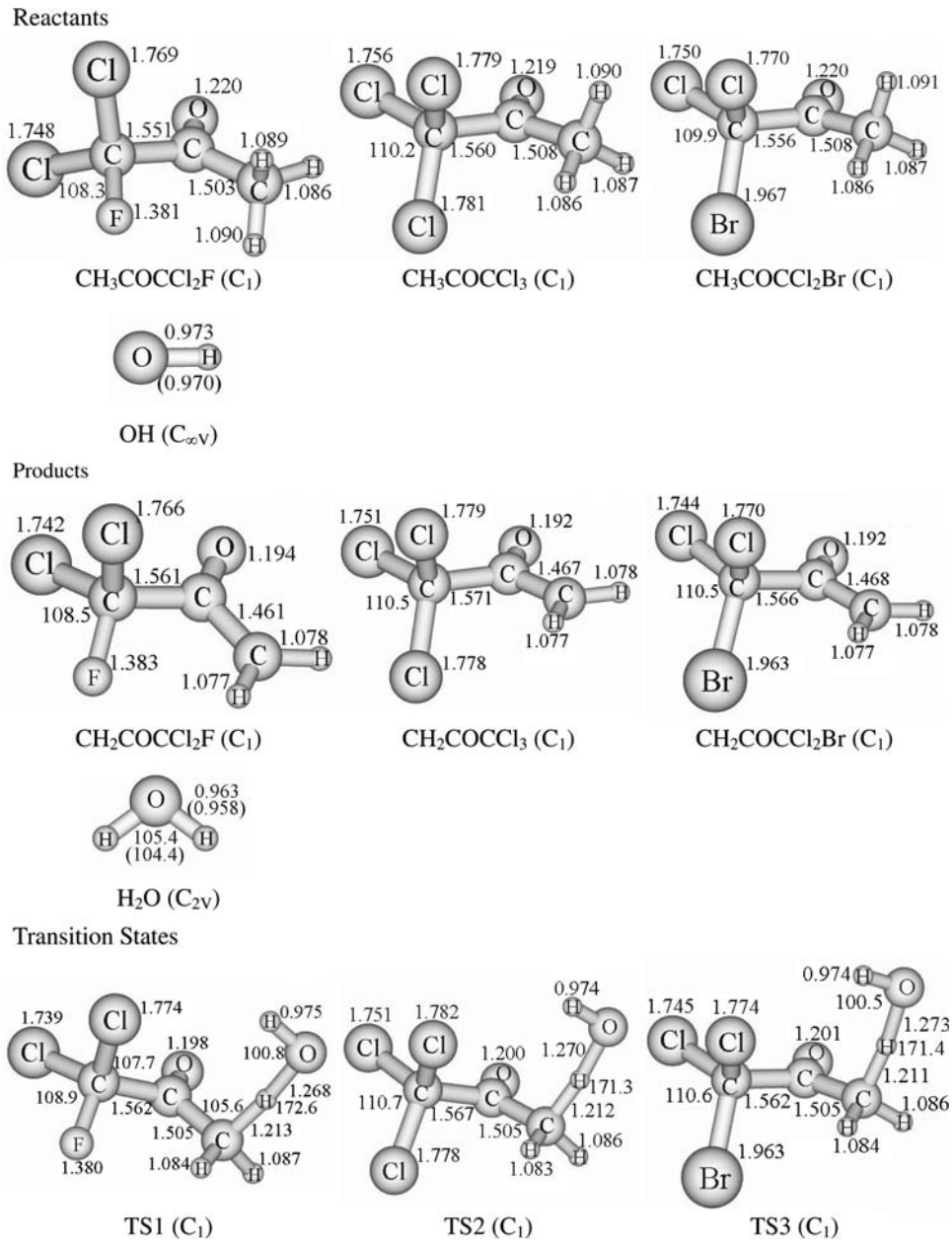

Fig. 1 Optimized geometries of the reactants, products, and saddle points at the MP2/6-31+G(d,p) level. The value in parentheses is the experimental value ([26] for OH and [27] for H_2O). Bond lengths are in angstroms, and bond angles are in degrees

CH_3COCCl_2F, CH_3COCCl_3, and CH_3COCCl_2Br; the forming bonds H–O stretch by 32, 32, and 32% over the equilibrium bond length in isolated molecule H_2O, respectively. The elongation of the forming bond is larger than that of the breaking bond, indicating that the barriers of reactions R1, R2, and R3 are near the corresponding reactants, and consequently, all of them will proceed reactant-like, i.e., the reactions will proceed via "early" transition state structures. Which is consistent with Hammond's postulate [28], applied to an exothermic hydrogen-abstraction reaction.

Table 1 lists the harmonic vibrational frequencies of all the stationary points for the reactants, products, and saddle points at the MP2/6-31+G(d,p) level as well as the corresponding available experimental results [9, 29, 30]. Our calculated frequencies are in agreement with the experimental values with the largest deviation within 6%. All the transition state structures in Table 1 are confirmed by normal-mode analysis to have one and only one imaginary frequency corresponding to the stretching modes of the coupling breaking and forming bonds. The values of these imaginary frequencies are $2{,}119i$ cm^{-1} for TS1, $2{,}085i$ cm^{-1} for TS2, and $2{,}061i$ cm^{-1} for TS3.

3.2 Energetics

The reaction enthalpies (ΔH^0_{298}) and potential barrier heights (ΔE^{TS}) with zero-point energy (ZPE) corrections

Table 1 Calculated and experimental frequencies (cm^{-1}) for the reactants, products, and saddle points at the MP2/6-31+G(d,p) level

Species	MP2/6-31+G(d,p)	Expt.
CH_3COCCl_2F	3,263, 3,225, 3,132, 1,783, 1,512, 1,508, 1,433, 1,266, 1,085, 1,069, 1,043, 921, 879, 613, 575, 544, 434, 380, 339, 279, 218, 180, 145, 45	
CH_3COCCl_3	3,267, 3,236, 3,139, 1,776, 1,521, 1,511, 1,434, 1,223, 1,066, 1,040, 901, 885, 813, 596, 570, 447, 407, 300, 291, 283, 193, 185, 123, 53	1,826, 849[a]
CH_3COCCl_2Br	3,264, 3,233, 3,136, 1,774, 1,518, 1,510, 1,434, 1,223, 1,065, 1,036, 898, 881, 751, 596, 546, 412, 396, 291, 244, 235, 186, 179, 133, 64	
OH	3,824	3,735[b]
H_2O	4,013, 3,866, 1,624	3,756, 3,657[c], 1,595
CH_2COCCl_2F	3,413, 3,274, 2,040, 1,500, 1,293, 1,081, 1,039, 942, 926, 775, 631, 595, 546, 436, 382, 347, 302, 277, 220, 178, 49	
CH_2COCCl_3	3,412, 3,275, 2,116, 1,505, 1,253, 1,031, 907, 893, 863, 728, 603, 596, 448, 410, 298, 294, 285, 248, 191, 169, 61	
CH_2COCCl_2Br	3,413, 3,275, 2,142, 1,501, 1,249, 1,031, 909, 888, 827, 700, 600, 589, 409, 402, 291, 283, 244, 234, 179, 150, 77	
TS1	3,803, 3,308, 3,202, 2,634, 1,495, 1,395, 1,294, 1,220, 1,085, 1,076, 1,029, 958, 907, 829, 730, 628, 584, 531, 435, 378, 357, 322, 280, 218, 175, 120, 81, 48, 26, 2,119*i*	
TS2	3,804, 3,307, 3,202, 2,548, 1,493, 1,397, 1,288, 1,204, 1,054, 1,019, 924, 894, 869, 799, 732, 602, 587, 447, 410, 356, 297, 290, 280, 193, 165, 137, 92, 56, 37, 2,085*i*	
TS3	3,805, 3,306, 3,201, 2,504, 1,491, 1,396, 1,288, 1,208, 1,048, 1,015, 923, 890, 855, 766, 722, 589, 575, 412, 398, 361, 289, 244, 234, 183, 146, 135, 96, 57, 40, 2,061*i*	

[a] Ref. [9]
[b] Ref. [29]
[c] Ref. [30]

Table 2 The reaction enthalpies at 298 K (ΔH^0_{298}) and the barrier height Va^G (kcal mol^{-1}) for the title reactions and CH_3COCH_3 reaction with OH at the MC-QCISD//MP2/6-31+G(d,p) level together with the experimental value

	MC-QCISD//MP2	Expt.
ΔH^0_{298}		
$OH + CH_3COCCl_2F \rightarrow CH_2COCCl_2F + H_2O$ (R1)	−23.21	
$OH + CH_3COCCl_3 \rightarrow CH_2COCCl_3 + H_2O$ (R2)	−23.30	
$OH + CH_3COCCl_2Br \rightarrow CH_2COCCl_2Br + H_2O$ (R3)	−22.98	
$OH + CH_3COCH_3 \rightarrow CH_2COCH_3 + H_2O$	−23.91	−23.89 ± 0.14
ΔVa^G		
$OH + CH_3COCCl_2F \rightarrow CH_2COCCl_2F + H_2O$ (R1)	4.98	
$OH + CH_3COCCl_3 \rightarrow CH_2COCCl_3 + H_2O$ (R2)	4.17	
$OH + CH_3COCCl_2Br \rightarrow CH_2COCCl_2Br + H_2O$ (R3)	4.04	

Experimental value derived from the standard heats of formation: OH, 9.33 kcal mol^{-1} [31]; CH_3COCH_3, −51.90 ± 0.14 kcal mol^{-1} [32]; CH_2COCH_3, −8.61 kcal mol^{-1} [33]; H_2O, −57.85 kcal mol^{-1} [31]

for reactions R1, R2, and R3 calculated at the MC-QCISD//MP2/6-31+G(d,p) level are listed in Table 2. It is shown that the three individual reactions are all exothermic, which is consistent with the discussion of Hammond's postulate [28]. Due to lack of the experimental heats of formation for the species involved in the title reactions, it is difficult to make a direct comparison between theory and experiment for the enthalpies of the three reactions. For comparison, the calculated reaction enthalpy of reaction CH_3COCH_3 with OH at the MC-QCISD//MP2/6-31+G(d,p) level as well as the available experimental reaction enthalpies is also listed in Table 2. The theoretical value of (ΔH^0_{298}) for the reaction of CH_3COCH_3 with OH is −23.91 kcal mol^{-1} which is in good agreement with the corresponding experimental value of −23.89 ± 0.14 kcal mol^{-1}, which was derived from the standard heats of formation (OH, 9.33 kcal mol^{-1} [31]; CH_3COCH_3, −51.90 ± 0.14 kcal mol^{-1} [32]; CH_2COCH_3, −8.61 kcal mol^{-1} [33]; H_2O,

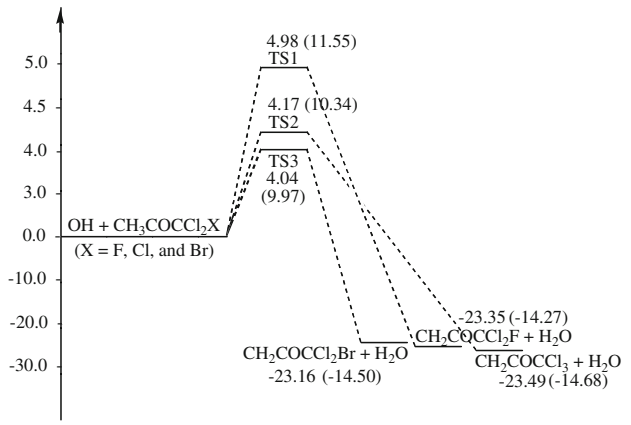

Fig. 2 Schematic potential energy surface for the title reactions. Relative energies (in kcal mol^{-1}) are calculated at the MC-QCISD//MP2/6-31+G(d,p) + ZPE level. The values in parentheses are calculated at the MP2/6-31+G(d,p) + ZPE level

−57.85 kcal mol^{-1} [31]). In view of the good agreement obtained above, it is expected that the enthalpies of the title reactions calculated at the same level are reliable.

A schematic potential energy diagram of the title reactions with ZPE corrections obtained at the MC-QCISD//MP2/6-31+G(d,p) level are described in Fig. 2. Note that the energy of the reactant is set to zero for reference. The values in parentheses are calculated at the MP2/6-31+G(d,p) level and include ZPE corrections. The barrier heights of reactions R1 (4.98 kcal mol^{-1}) and R2 (4.17 kcal mol^{-1}) are about 0.9 and 0.1 kcal mol^{-1} higher than that of reaction R3 (4.04 kcal mol^{-1}), respectively. And as a result, the latter reaction path R3 is more kinetically favorable than the two former, it is expected to have larger rate constants.

3.3 Rate constants

Dual-level dynamics [10–12] calculations of the OH + CH_3COCCl_2X (X = F, Cl, and Br) reactions are carried out at the MC-QCISD//MP2/6-31+G(d,p) level. The rate constants, k_1 for R1, k_2 for R2, and k_3 for R3, are evaluated by conventional transition state theory (TST), the ICVT, and the ICVT with the SCT contributions in a wide temperature range from 200 to 3,000 K. The calculated rate constants TST, ICVT, and ICVT/SCT of the three reactions are displayed in Table 3. From Table 3, it is shown that for the reactions R1, R2, and R3, the tunneling effect, i.e., the ratio between ICVT and ICVT/SCT rate constants, plays a significant role in the temperature range 200–600 K. The ratios of k_1(ICVT/SCT)/k_1(ICVT) are 14.29, 1.89, and 1.32 at 200, 400, and 600 K for R1, 3.13, 1.41, and 1.16 at 200, 400, and 600 K for R2, 8.33, 1.52, and 1.19 at 200, 400, and 600 K for R3, respectively. While the variational effect, i.e., the ratio between ICVT and TST rate constants, [k(ICVT)/k(TST)], for R1 reaction, the variational effect ranges from 0.94 (200 K) to 0.31 (3,000 K), and for R2 and R3 reaction, the corresponding with variational effect ranges from 0.95 to 0.50, and from 0.97 to 0.49, respectively. The theoretical ICVT/SCT rate constant of reaction R1 is 1.60×10^{-15} $cm^3molecule^{-1}$ s^{-1}, which is smaller than those of reactions R2 (1.68×10^{-14} $cm^3molecule^{-1}$ s^{-1}) and R3 (4.57×10^{-14} $cm^3molecule^{-1}$ s^{-1}) at 298 K. Theoretical activation energy (E_a) is estimated based on the calculated CVT/SCT rate constants, and it is found that the corresponding E_a value for reaction R3, 4.32 kcal mol^{-1}, is lower than that for reactions R2 (5.08 kcal mol^{-1}) and R1 (5.43 kcal mol^{-1}) in 200–600 K.

The ICVT/SCT rate constants for the three reactions OH + CH_3COCCl_2F → CH_2COCCl_2F + H_2O (k_1), OH + CH_3COCCl_3 → CH_2COCCl_3 + H_2O (k_2), and OH + CH_3COCCl_2Br → CH_2COCCl_2Br + H_2O (k_3) are plotted against the reciprocal of temperature in Fig. 3 as well as the corresponding experimental data [9]. The ICVT/SCT rate constant of k_2, 1.68×10^{-14} $cm^3molecule^{-1}$ s^{-1}, is in good agreement with the corresponding experimental one, $(1.5 \pm 0.3) \times 10^{-14}$ $cm^3molecule^{-1}$ s^{-1}, given by Carr et al. [9] at 298 K. The deviation between the theoretical and experimental values remains within a factor of approximately 1.12. Thus, the present calculations may provide a reliable prediction of the rate constants for the title reactions over the wide temperature range.

Seen from Fig. 3, the rate constants of reaction R3 are about 1–7 times larger than that of reaction R2 and first order of magnitude larger than those of reaction R1 from 200 to 3,000 K, respectively. This is consistent with a qualitative assessment based on the potential energy barrier heights and the reaction enthalpies of these three reactions.

As a result of the limited experimental knowledge of the kinetic nature of the title reactions, we hope that our present study may provide useful information for future laboratory investigations. For convenience of future experimental measurements, the three-parameter fits for the ICVT/SCT rate constants of the title reactions in the temperature range 200–3,000 K are performed and the expressions are given as follows: (in unit of $cm^3molecule^{-1}$ s^{-1})

$$k_1(T) = 1.97 \times 10^{-20} T^{2.85} \exp(-1447.23/T)$$

$$k_2(T) = 8.18 \times 10^{-18} T^{2.33} \exp(-1687.48/T)$$

$$k_3(T) = 7.66 \times 10^{-19} T^{2.68} \exp(-1250.26/T).$$

4 Conclusions

In this paper, the title reactions OH + CH_3COCCl_2X → products (X = F, Cl, and Br) have been studied by

Table 3 The TST, ICVT and ICVT/SCT rate constants calculated at the MC-QCISD//MP2/6-31+G(d,p) level for three reactions, R1, R2, and R3, between 200 and 3,000 K ($cm^3 molecule^{-1} s^{-1}$)

T(K)	$OH + CH_3COCCl_2F \rightarrow CH_2COCCl_2F + H_2O$ (R1)			$OH + CH_3COCCl_3 \rightarrow CH_2COCCl_3 + H_2O$ (R2)			$OH + CH_3COCCl_2Br \rightarrow CH_2COCCl_2Br + H_2O$ (R3)		
	TST	ICVT	ICVT/SCT	TST	ICVT	ICVT/SCT	TST	ICVT	ICVT/SCT
200	4.05×10^{-18}	3.79×10^{-18}	5.63×10^{-17}	1.32×10^{-16}	1.26×10^{-16}	3.95×10^{-16}	3.20×10^{-16}	3.09×10^{-16}	2.59×10^{-15}
250	8.31×10^{-17}	7.63×10^{-17}	3.96×10^{-16}	1.76×10^{-15}	1.66×10^{-15}	3.62×10^{-15}	3.99×10^{-15}	3.79×10^{-15}	1.28×10^{-14}
298	6.12×10^{-16}	5.10×10^{-16}	1.60×10^{-15}	9.84×10^{-15}	9.45×10^{-15}	1.68×10^{-14}	2.13×10^{-14}	2.06×10^{-14}	4.57×10^{-14}
350	3.01×10^{-15}	2.31×10^{-15}	5.28×10^{-15}	3.90×10^{-14}	3.69×10^{-14}	5.67×10^{-14}	8.18×10^{-14}	7.88×10^{-14}	1.37×10^{-13}
400	9.79×10^{-15}	7.01×10^{-15}	1.32×10^{-14}	1.09×10^{-13}	9.96×10^{-14}	1.40×10^{-13}	2.23×10^{-13}	2.04×10^{-13}	3.09×10^{-13}
450	2.54×10^{-14}	1.70×10^{-14}	2.80×10^{-14}	2.50×10^{-13}	2.21×10^{-13}	2.89×10^{-13}	5.02×10^{-13}	4.45×10^{-13}	6.11×10^{-13}
500	5.58×10^{-14}	3.53×10^{-14}	5.29×10^{-14}	5.01×10^{-13}	4.27×10^{-13}	5.33×10^{-13}	9.87×10^{-13}	8.46×10^{-13}	1.09×10^{-12}
550	1.09×10^{-13}	6.55×10^{-14}	9.16×10^{-14}	9.04×10^{-13}	7.47×10^{-13}	8.98×10^{-13}	1.76×10^{-12}	1.46×10^{-12}	1.80×10^{-12}
600	1.95×10^{-13}	1.11×10^{-13}	1.47×10^{-13}	1.51×10^{-12}	1.21×10^{-12}	1.41×10^{-12}	2.91×10^{-12}	2.34×10^{-12}	2.79×10^{-12}
650	3.23×10^{-13}	1.77×10^{-13}	2.25×10^{-13}	2.37×10^{-12}	1.85×10^{-12}	2.11×10^{-12}	4.52×10^{-12}	3.54×10^{-12}	4.10×10^{-12}
800	1.09×10^{-12}	5.37×10^{-13}	6.30×10^{-13}	7.03×10^{-12}	5.10×10^{-12}	5.58×10^{-12}	1.32×10^{-11}	9.57×10^{-12}	1.05×10^{-11}
1,000	3.54×10^{-12}	1.56×10^{-12}	1.73×10^{-12}	2.03×10^{-11}	1.37×10^{-11}	1.45×10^{-11}	3.74×10^{-11}	2.51×10^{-11}	2.66×10^{-11}
1,500	2.26×10^{-11}	8.48×10^{-12}	8.87×10^{-12}	1.10×10^{-10}	6.51×10^{-11}	6.68×10^{-11}	1.98×10^{-10}	1.16×10^{-10}	1.19×10^{-10}
2,000	7.10×10^{-11}	2.42×10^{-11}	2.47×10^{-11}	3.10×10^{-10}	1.71×10^{-10}	1.73×10^{-10}	5.54×10^{-10}	3.00×10^{-10}	3.05×10^{-10}
2,400	1.38×10^{-10}	4.46×10^{-11}	4.53×10^{-11}	5.66×10^{-10}	2.99×10^{-10}	3.02×10^{-10}	1.01×10^{-9}	5.21×10^{-10}	5.26×10^{-10}
3,000	2.94×10^{-10}	9.01×10^{-11}	9.11×10^{-11}	1.12×10^{-9}	5.64×10^{-10}	5.68×10^{-10}	1.98×10^{-9}	9.75×10^{-10}	9.82×10^{-10}

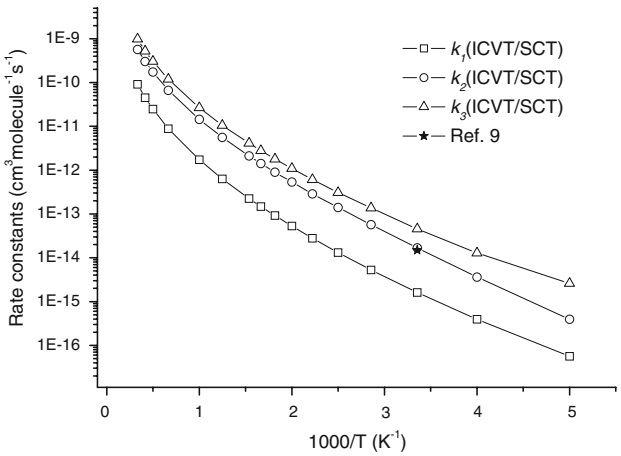

Fig. 3 The ICVT/SCT rate constants calculated at the MC-QCISD//MP2/6-31+G(d,p) level for three reactions, R1 (k_1), R2 (k_2) and R3 (k_3) (in $cm^3molecule^{-1}\ s^{-1}$), versus 1,000/$T$ between 200 and 3,000 K, together with the experimental value

theoretical methods. The potential energy surface information is obtained at the MP2/6-31+G(d,p) level, and higher-level energies for the stationary points and a few extra points along the minimum energy path are further refined by the MC-QCISD theory. The theoretical rate constants are calculated by ICVT incorporating the SCT contributions method in the temperature range 200–3,000 K. The calculated rate constant k_2 is in good agreement with the available experimental value. Given the good agreement between the theoretical and experimental values, it is reasonable to believe that our calculated results will provide a good estimate for the kinetics of the reactions in the high temperature range.

Acknowledgments The authors thank Professor Donald G. Truhlar for providing the POLYRATE 9.1 program. This work is supported by the National Natural Science Foundation of China (20333050, 20303007, 50743013, and 20272011), the program for New Century Excellent Talents in University (NCET), the Doctor Foundation by the Ministry of Education, the Foundation for University Key Teacher by the Department of Education of Heilongjiang Province (1151G019, 1152G010), the key subject of Science and Technology by the Ministry of Education of China, the key subject of Science and Technology by Jilin Province, the SF for leading experts in academe of Harbin of China (2007RFXXG027), the SF for Postdoctoral of Heilongjiang province of China (LBH-Q07058), and Natural Science Foundation of Heilongjiang Province (TA2005-15, B200605).

References

1. Singh HB, O'Hara D, Herlth D, Sachse W, Blake DR, Bradshaw JD, Kanakidou M, Crutzen PJ (1994) J Geophys Res 99:1805. doi:10.1029/93JD00764
2. Singh HB, Kanakidou M, Crutzen PJ, Jacob DJ (1995) Nature 378:50. doi:10.1038/378050a0
3. Arnold F, Knop G, Zierens H (1986) Nature 321:505. doi:10.1038/321505a0
4. Arnold F, Burger V, Drost-Fanke B, Grimm F, Schneider J, Krieger A, Stile T (1997) Geophys Res Lett 24:3017. doi:10.1029/97GL02974
5. Martínez E, Aranda A, Díaz-de-Mera Y, Rodríguez A, Rodríguez D, Notario A (2004) J Atmos Chem 48:283. doi:10.1023/B:JOCH.0000044424.22309.d8
6. El-Nahas AM, Bozzelli JW, Simmie JM, Navarro MV, Black G, Curran HJ (2006) J Phys Chem A 110:13618. doi:10.1021/jp065003y
7. Hou H, Li YZ, Wang BS (2006) J Phys Chem A 110:13163. doi:10.1021/jp065346w
8. Caralp F, Forst W, Henon E, Bergeata A, Bohr F (2006) Phys Chem Chem Phys 8:1072. doi:10.1039/b515118j
9. Carr S, Shallcross DE, Canosa-Mas CE, Wenger JC, Sidebottom HW, Treacy JJ, Wayne RP (2003) Phys Chem Chem Phys 5:3874. doi:10.1039/b304298g
10. Truhlar DG (1995) In: Heidrich D (ed) The reaction path in chemistry: current approaches and perspectives. Kluwer, Dordrecht, p 229
11. Truhlar DG, Garrett BC, Klippenstein SJ (1996) J Phys Chem 100:12771. doi:10.1021/jp953748q
12. Hu W-P, Truhlar DG (1996) J Am Chem Soc 118:860. doi:10.1021/ja952464g
13. Fast PL, Truhlar DG (2000) J Phys Chem A 104:6111. doi:10.1021/jp000408i
14. Corchado JC, Chuang Y-Y, Fast PL, Villa J, Hu W-P, Liu Y-P, Lynch GC, Nguyen KA, Jackels CF, Melissas VS, Lynch BJ, Rossi I, Coitino EL, Ramos AF, Pu J, Albu TV (2002) POLYRATE version 9.1. Department of Chemistry and Supercomputer Institute, University of Minnesota, Minneapolis, Minnesota
15. Truhlar DG, Garrett BC (1980) Acc Chem Res 13:440. doi:10.1021/ar50156a002
16. Truhlar DG, Isaacson AD, Garrett BC (1985) Generalized transition state theory. In: Baer M (ed) The theory of chemical reaction dynamics, vol 4. CRC Press, Boca Raton, p 65
17. Duncan WT, Truong TN (1995) J Chem Phys 103:9642. doi:10.1063/1.470731
18. Frisch MJ, Head-Gordon M, Pople JA (1990) Chem Phys Lett 166:275. doi:10.1016/0009-2614(90)80029-D
19. Head-Gordon M, Pople JA, Frisch MJ (1988) Chem Phys Lett 153:503. doi:10.1016/0009-2614(88)85250-3
20. Frisch MJ, Trucks GW, Schlegel HB, Scuseria GE, Robb MA, Cheeseman JR, Montgomery JA Jr, Vreven T, Kudin KN, Burant JC, Millam JM, Iyengar SS, Tomasi J, Barone V, Mennucci B, Cossi M, Scalmani G, Rega N, Petersson GA, Nakatsuji H, Hada M, Ehara M, Toyota K, Fukuda R, Hasegawa J, Ishida M, Nakajima T, Honda Y, Kitao O, Nakai H, Klene M, Li X, Knox JE, Hratchian HP, Cross JB, Adamo C, Jaramillo J, Gomperts R, Stratmann RE, Yazyev O, Austin AJ, Cammi R, Pomelli C, Ochterski JW, Ayala PY, Morokuma K, Voth GA, Salvador P, Dannenberg JJ, Zakrzewski VG, Dapprich S, Daniels AD, Strain MC, Farkas O, Malick DK, Rabuck AD, Raghavachari K, Foresman JB, Ortiz JV, Cui Q, Baboul AG, Clifford S, Cioslowski J, Stefanov BB, Liu G, Liashenko A, Piskorz P, Komaromi I, Martin RL, Fox DJ, Keith T, Al-Laham MA, Peng CY, Nanayakkara A, Challacombe M, Gill PMW, Johnson B, Chen W, Wong MW, Gonzalez C, Pople JA (2003) Gaussian, Inc., Pittsburgh, PA
21. Garrett BC, Truhlar DG, Grev RS, Magnuson AW (1980) J Phys Chem 84:1730. doi:10.1021/j100450a013
22. Lu DH, Truong TN, Melissas VS, Lynch GC, Liu YP, Grarrett BC, Steckler R, Issacson AD, Rai SN, Hancock GC, Lauderdale JG, Joseph T, Truhlar DG (1992) Comput Phys Commun 71:235. doi:10.1016/0010-4655(92)90012-N
23. Liu Y-P, Lynch GC, Truong TN, Lu D-H, Truhlar DG, Garrett BC (1993) J Am Chem Soc 115:2408. doi:10.1021/ja00059a041

24. Truhlar DG (1991) J Comput Chem 12:266. doi:10.1002/jcc.540120217
25. Chuang YY, Truhlar DG (2000) J Chem Phys 112:1221. doi:10.1063/1.480768
26. In NIST Chemistry WebBook, NIST Standard Reference Database Number 69, June 2005 Release (Constants of Diatomic Molecules date compiled by K. P. Huber and G. Herzberg)
27. Kuchitsu K (1998) In: Structure of free polyatomic molecules basic data, vol 1. Springer-Verlag, Berlin, p 58
28. Hammond GS (1955) J Am Chem Soc 77:334. doi:10.1021/ja01607a027
29. Shimanouchi T (1972) In: Tables of molecular vibrational frequencies consolidated, vol 1. National Bureau of Standards, U.S. GPO, Washinton
30. In NIST Chemistry WebBook, NIST Standard Reference Database Number 69, June 2005 Release (Vibrational frequency date compiled by T. Shimanouchi)
31. Chase MW Jr (1998) NIST-JANAF Themochemical tables, 4th edn. J Phys Chem Ref Data Monogr 9:1–1951
32. Wiberg KB, Crocker LS, Morgan KM (1991) Thermochemical studies of carbonyl compounds. 5. Enthalpies of reduction of carbonyl groups. J Am Chem Soc 113:3447. doi:10.1021/ja00009a033
33. Burcat A, McBride B (1997) Ideal gas thermodynamic data for combustion and air-pollution use, Technion Aerospace Engineering (TAE) Report # 804 June 1997